



Effect of cerium addition on non-metallic inclusions in a high-carbon chromium bearing steel

Hao Li¹ · Qiang Ren² · Li-feng Zhang³

Received: 2 September 2022 / Revised: 25 September 2022 / Accepted: 29 September 2022 / Published online: 21 January 2023
© China Iron and Steel Research Institute Group 2023

Abstract

Effects of varied levels of cerium (28×10^{-6} , 65×10^{-6} and 150×10^{-6}) on inclusions in a high-carbon chromium bearing steel at different stages (before adding cerium, after adding cerium for 1, 5, 10 min and ingot) were studied using laboratory experiments. An automatic scanning electron microscope system with energy-dispersive spectroscopy was used to analyze the amount, composition, size and morphology of inclusions in the steel at different stages. When the cerium content in the molten steel increased from 0 to 150×10^{-6} , the evolution sequence of inclusions was as follows: $\text{Al}_2\text{O}_3 \rightarrow \text{CeAl}_{11}\text{O}_{18} \rightarrow \text{CeAlO}_3 \rightarrow \text{Ce}_2\text{O}_2\text{S}$. After 28×10^{-6} cerium was added, Al_2O_3 inclusions were modified into $\text{CeAl}_{11}\text{O}_{18}$ inclusions in the molten steel and then were further transformed into Al_2O_3 and CeAlO_3 inclusions in the solid steel during cooling. With the addition of 65×10^{-6} cerium, inclusions in the molten steel were modified into CeAlO_3 and a small number of $\text{Ce}_2\text{O}_2\text{S}$ inclusions. When the addition amount of cerium increased to 150×10^{-6} , inclusions were transformed to $\text{Ce}_2\text{O}_2\text{S}$. The size of inclusions in the molten steel decreased obviously with cerium addition. On the other hand, the size of inclusions increased during the cooling process in solid steels of No. 1 steel (with 28×10^{-6} cerium) and No. 2 steel (with 65×10^{-6} cerium). During the cooling process, unmodified MnS inclusions were precipitated in the solid steel of No. 1 steel and wrapped outside the Al_2O_3 and CeAlO_3 inclusions to form large complex inclusions. During the cooling process of No. 2 steel, the inclusion size of CeAlO_3 increased due to the collision and polymerization. In the No. 3 steel (with 150×10^{-6} cerium), the average size of inclusions decreased rapidly and remained at a lower size during the cooling process, which was beneficial to improving the fatigue life of the steel.

Keywords Cerium · Inclusion · Transformation · High-carbon chromium bearing steel · Modification

1 Introduction

The high-carbon chromium bearing steel is commonly used as the manufacturing material of mechanical bearings, which is widely used in high-speed railways, aerospace

equipment, military weapons and other industrial machinery fields. Bearings usually work under good lubrication conditions with a stress load less than their yield strength; thus, the main failure of bearings was subsurface fatigue failure [1, 2], and one of the sources of subsurface fatigue failure of bearing steel was non-metallic inclusions. The amount, composition, size, morphology and spatial distribution of inclusions were of great importance for the fatigue life of high-strength steels [3–10]. Improving the control of non-metallic inclusions favors the fatigue performance of the bearing steel.

Rare earth metals have been used to purify the molten steel and modify inclusions due to their strong affinity with oxygen, sulfur and other elements in the steel [11–14]. Alumina inclusions are the common inclusions in the high-carbon chromium bearing steel and are detrimental to fatigue properties of the steel [15–17]. Hence, rare earth

✉ Qiang Ren
renqiang@ysu.edu.cn

✉ Li-feng Zhang
zhanglifeng@ncut.edu.cn

¹ State Key Lab of Metastable Materials Science and Technology, Yanshan University, Qinhuangdao 066004, Hebei, China

² School of Mechanical Engineering, Yanshan University, Qinhuangdao 066004, Hebei, China

³ School of Mechanical and Materials Engineering, North China University of Technology, Beijing 100144, China

metals can improve the fatigue performance of the steel if inclusions in the steel were modified into less detrimental ones. Rare earth metals have been widely used to modify inclusions in steels [18–23]. Ren and Zhang [13] proposed a $\text{Al}_2\text{O}_3 \rightarrow \text{CeAlO}_3 \rightarrow \text{Ce}_2\text{O}_2\text{S} \rightarrow \text{Ce}_2\text{O}_2\text{S} + \text{CeS}$ modification sequence of inclusions in a ultra-low-carbon Al-killed steel by cerium addition. Wang et al. [24] reported a $\text{Al}_2\text{O}_3 \rightarrow \text{CeAl}_{11}\text{O}_{18} \rightarrow \text{CeAlO}_3 \rightarrow \text{Ce}_2\text{O}_2\text{S}$ evolution sequence of inclusions in an H13 hot working abrasive steel by varied levels of cerium in the steel. There were studies on the effect of rare earth metals on properties of the bearing steel [25, 26]; however, the evolution of inclusions in the molten high-carbon chromium bearing steel and in the solid steel during cooling by varied additions of rare earth metals was hardly reported.

In the current work, the cerium metal was used as modifier of inclusions in a high-carbon chromium bearing steel. The effect of the addition amount of cerium on inclusions in the molten steel and in the solid steel during the cooling process was studied. A thermodynamic calculation was performed to achieve the phase transformation of inclusions to support the experimental observation. The current paper is to provide a useful reference for the proper use of cerium metal in the bearing steel to achieve a better fatigue performance.

2 Laboratory experiments and analysis

To obtain high-carbon chromium bearing steels with varied cerium contents, approximately 600 g of surface-polished and cleaned billet samples was melted in an alumina crucible in a MoSi_2 resistance furnace purged with pure argon gas. As shown in Fig. 1, after the steel was heated to

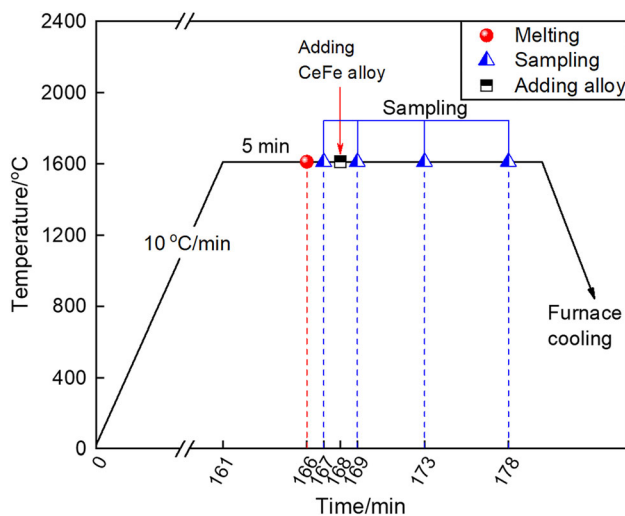


Fig. 1 Steel melting and sampling during each experiment

1610 °C and held for 5 min, CeFe (20 wt.% Ce) alloy was added into the molten steel. Three steel samples at 1, 5 and 10 min after the addition of cerium ferroalloy were taken with a quartz sampler and were quenched in water. The remaining molten steel was cooled in the furnace to room temperature in order to study the stronger transformation of inclusions during steel cooling since the smaller cooling rate led to more transformation of inclusions in the steel than the larger cooling rate [27].

The machining of molten steel samples is shown in Fig. 2. Inclusions on the cross section of the sample at 10 mm above the bottom were detected, above which a 20-mm-high rod with a 5 mm diameter was machined to detect the total oxygen (TO) and the total nitrogen (TN) of the steel. Machined steel chips were used to analyze the total cerium (TCe) content and the total sulfur (TS) content in the steel. The machining of steel ingot samples cooled in the furnace is shown in Fig. 3. A 7-mm-diameter rod at 5 mm away from ingot edge was machined to detect TO and TN of the steel, and a 10 mm × 10 mm × 5 mm cube at 16 mm away from ingot edge and 10 mm beneath ingot top was sampled to detect inclusions in the steel. Machined steel chips were used to detect TCe and TS in the steel.

Table 1 shows the chemical composition of the high-carbon chromium bearing steel billet, which was analyzed using a direct reading spectrometer. Table 2 shows the chemical composition of quenched samples and ingot samples. The cerium content in the steel was measured using an inductively coupled plasma mass spectrometer. Contents of oxygen, nitrogen and sulfur in the steel were measured using a LECO oxygen and nitrogen analyzer and a LECO carbon and sulfur analyzer. For the inclusion analysis, the backscattered electron probe of scanning electron microscope (SEM) was used to distinguish the contrast between the steel matrix and inclusions after polishing. The composition, size, amount and morphology of inclusions larger than 1 μm were detected with a 20 kV accelerating voltage and a 350 magnification during the automated scanning process. During statistical analysis of

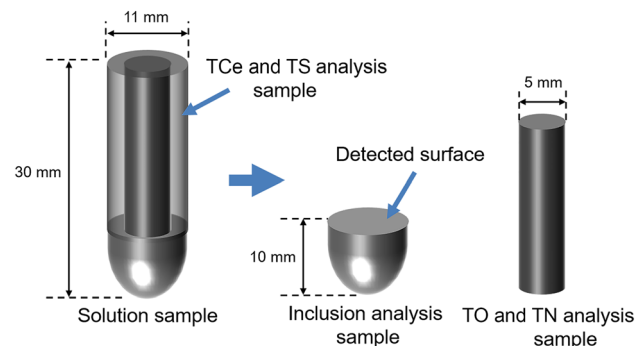


Fig. 2 Machining and detection plan of molten steel samples

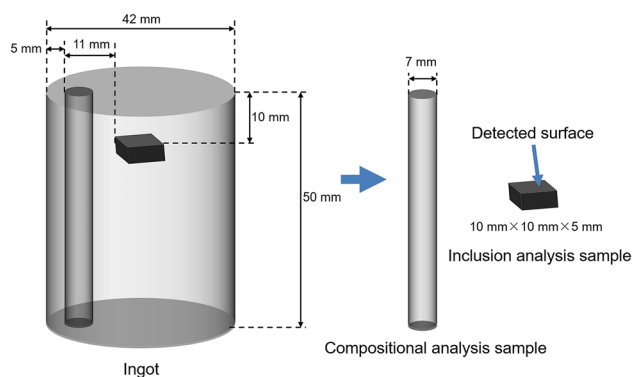


Fig. 3 Machining and detection plan of ingot steel samples

inclusions, dust and impurities in the original SEM data were removed.

3 Evolution of inclusions in steel during cerium modification

3.1 Evolution of inclusions composition in molten steel

Before the addition of the cerium ferroalloy, the composition and size statistic of inclusions in the molten steel were projected in the CaO–MgO–Al₂O₃ ternary diagram,

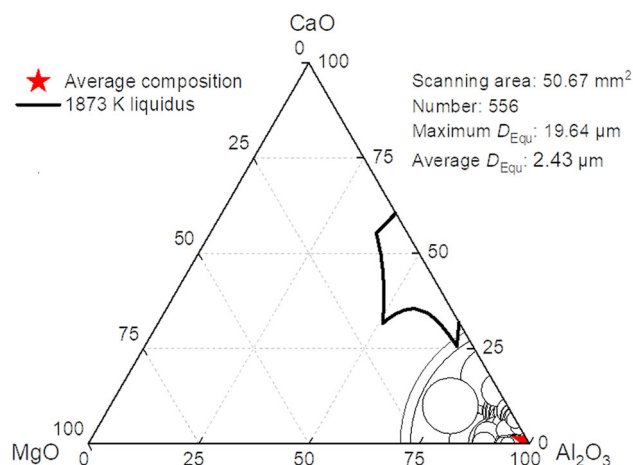


Fig. 4 Composition and size distributions of inclusions before cerium addition in molten steel. D_{Equ} —Equivalent circular diameter of inclusion area

as shown in Fig. 4. The size of the circle represented the diameter of the inclusion, and the red five-pointed star indicated the average composition of inclusions in the molten steel. Inclusions in the steel were primarily composed of Al₂O₃ and a few Al₂O₃–CaO. The elemental mapping of typical inclusions in the steel is shown in Fig. 5, and the Al₂O₃ and Al₂O₃–CaO inclusions were both in angular shape, indicating that initial inclusions in the molten bearing steel were in solid state.

Table 1 Chemical composition of commercial high-carbon chromium bearing steel billets (wt.%)

C	Si	Mn	Cr	Al	Mg	Ca	Ti	O
0.99	0.23	0.3	1.47	0.012	0.0005	0.0002	0.0013	0.0005

Table 2 Main chemical composition of molten samples and ingot samples

No.	Holding time/min	TCe	TO	TS
1	1	28×10^{-6}	22.5×10^{-6}	45.8×10^{-6}
	5	28×10^{-6}	22.6×10^{-6}	38.7×10^{-6}
	10	28×10^{-6}		42.9×10^{-6}
	Ingot	28×10^{-6}	18.2×10^{-6}	40.8×10^{-6}
2	1	65×10^{-6}	26.9×10^{-6}	49.1×10^{-6}
	5	63×10^{-6}		45.9×10^{-6}
	10	66×10^{-6}		44.1×10^{-6}
	Ingot	65×10^{-6}	20.2×10^{-6}	42.1×10^{-6}
3	1	150×10^{-6}	22.5×10^{-6}	47.7×10^{-6}
	5	150×10^{-6}	22.9×10^{-6}	43.5×10^{-6}
	10	150×10^{-6}	22.1×10^{-6}	43.6×10^{-6}
	Ingot	150×10^{-6}	21.3×10^{-6}	44.3×10^{-6}

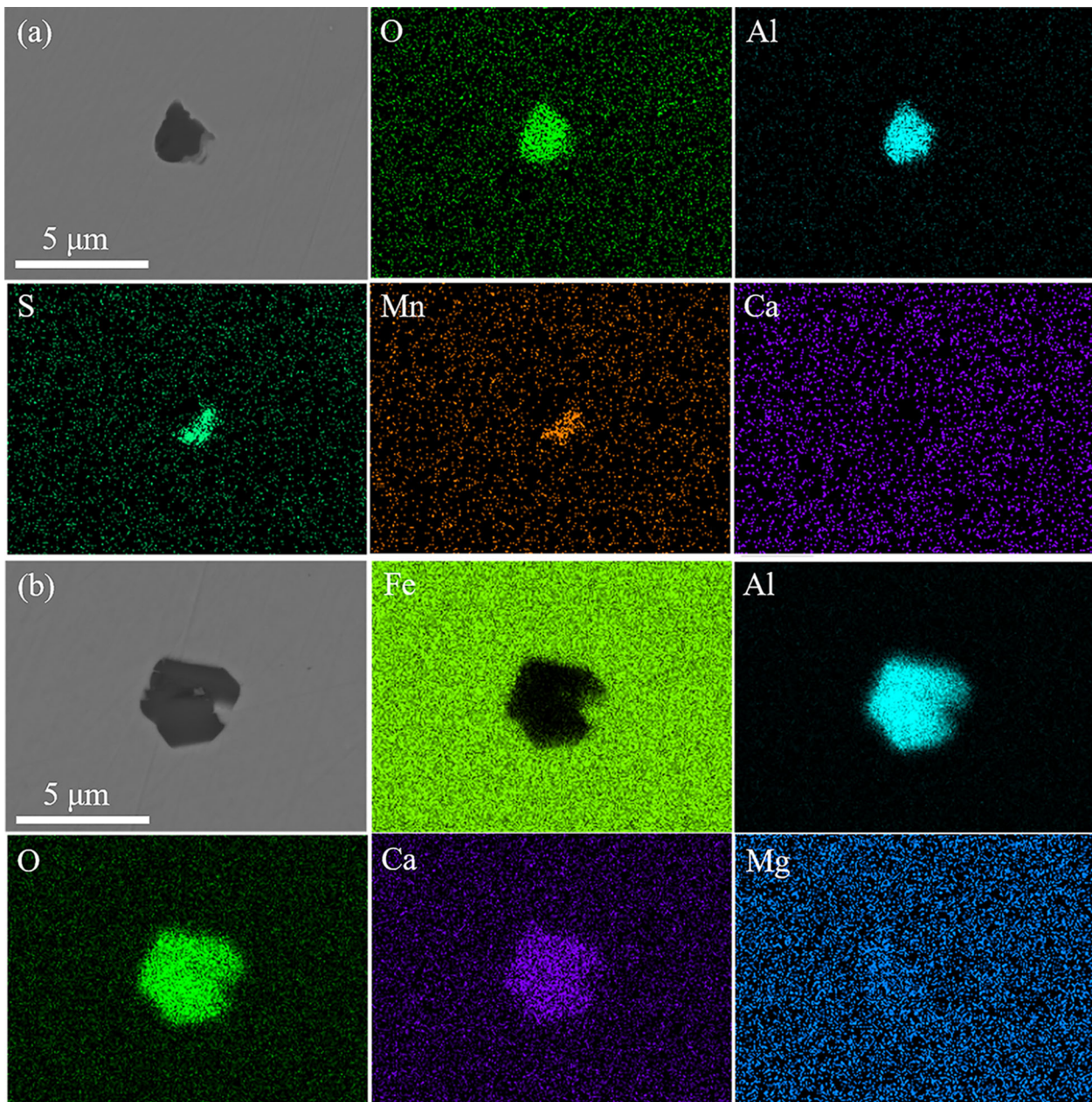


Fig. 5 Typical inclusions in molten steel before cerium addition. **a** Al_2O_3 -MnS complex inclusion; **b** Al_2O_3 -CaO inclusion

According to energy-dispersive spectroscopy (EDS) analysis results, statistics of inclusions composition and size in No. 1 steel were performed and projected in Ce-Al-O-S diagram, where the positions of CeAlO_3 , $\text{Ce}_2\text{O}_2\text{S}$ and CeS were determined by atomic ratios and were marked by red arrows, as shown in Fig. 6. One minute after the cerium ferroalloy was added, a large number of Al_2O_3 (-CaO) inclusions were immediately modified to $\text{CeAl}_{11}\text{O}_{18}$ (-CaO) inclusions (as shown in Fig. 7b). However, a small part of initial inclusions was unmodified (as shown in Fig. 7a). Five minutes after the addition of the cerium ferroalloy, a small number of CeAlO_3 (-CaO) inclusions

were generated in the molten steel (as shown in Fig. 7c), and the amount of CeAlO_3 (-CaO) was slightly increased 10 min after the addition of cerium, which was due to the uneven distribution of cerium in the molten steel. To be concluded, after the addition of 28×10^{-6} cerium in the molten steel, the modification of Al-O inclusions into Al-Ce-O inclusions was the main reaction, in which calcium did not participate in the reaction.

Figure 8 shows the statistics of inclusions composition and size in No. 2 steel. After CeFe alloy was added for 1 min, main inclusions in the molten steel were CeAlO_3 (-CaO) inclusions, and a small number of $\text{Ce}_2\text{O}_2\text{S}$

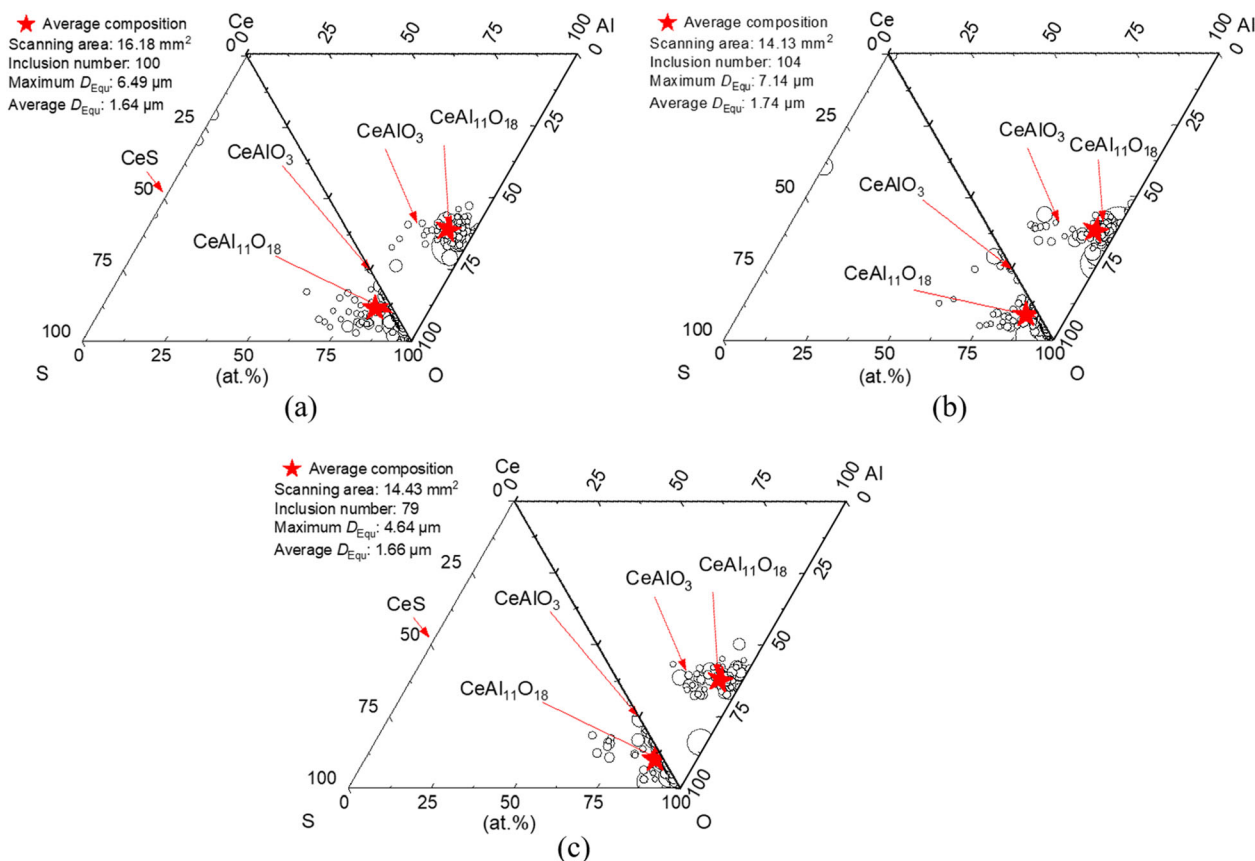


Fig. 6 Composition and size of inclusions at different time after cerium addition in No. 1 steel. **a** 1 min; **b** 5 min; **c** 10 min

inclusions were generated. Then, the number of $\text{Ce}_2\text{O}_3\text{S}$ inclusions increased with time. Statistic of the calcium content of inclusions in the steel is shown in Fig. 9, and with the addition of 28×10^{-6} cerium (No. 1 steel), the calcium content of inclusions decreased slightly. When the addition amount of cerium increased to 65×10^{-6} (No. 2 steel), the calcium content of inclusions gradually decreased with time. As for the addition of 150×10^{-6} cerium (No. 3 steel), there was almost no calcium element in inclusions. Elemental mappings of typical inclusions in the No. 2 molten steel after the cerium addition are shown in Fig. 10, and there was a certain amount of calcium in the inclusion after the cerium addition for 1 and 5 min; however, calcium disappeared at 10 min after the cerium addition, indicating that calcium in CeAlO_3 (-CaO) inclusions was reduced to the molten steel as dissolved calcium.

As shown in Fig. 11, five minutes after the addition of 150×10^{-6} cerium in the molten steel, a small number of $\text{Ce}_2\text{O}_3\text{S}$ and Ce_xS_y complex inclusions were observed, as shown in Fig. 12a. The content of Ce_xS_y inclusions gradually decreased at 10 min after the addition of cerium, which meant that Ce_xS_y inclusions were transiently generated due to the formation of a cerium-enriched region in the molten steel at the initial stage. The composition of the

molten steel was gradually homogenized with time, and the composition of inclusions in the molten steel finally stabilized near the $\text{Ce}_2\text{O}_3\text{S}$, as shown in Fig. 12b.

3.2 Evolution of inclusion composition during solidification

The composition and size of inclusions in solid steels with varied cerium contents are shown in Fig. 13. By comparing Figs. 6c and 13a, inclusions in No. 1 steel changed from $\text{CeAl}_{11}\text{O}_{18}$ to CeAlO_3 and Al_2O_3 during the cooling process, as shown in Fig. 14a. However, in No. 2 and No. 3 steels, the composition of inclusions did not change during the cooling process, as shown in Fig. 13b and c. Typical inclusions in the solidified ingot are shown in Fig. 14b and c.

4 Evolution of inclusions size and number density

Figure 15 shows the variation of the average size and number density of inclusions with the addition of cerium. As shown in Fig. 15a, because the large Ca-Al-O inclusions were modified into small cerium-containing

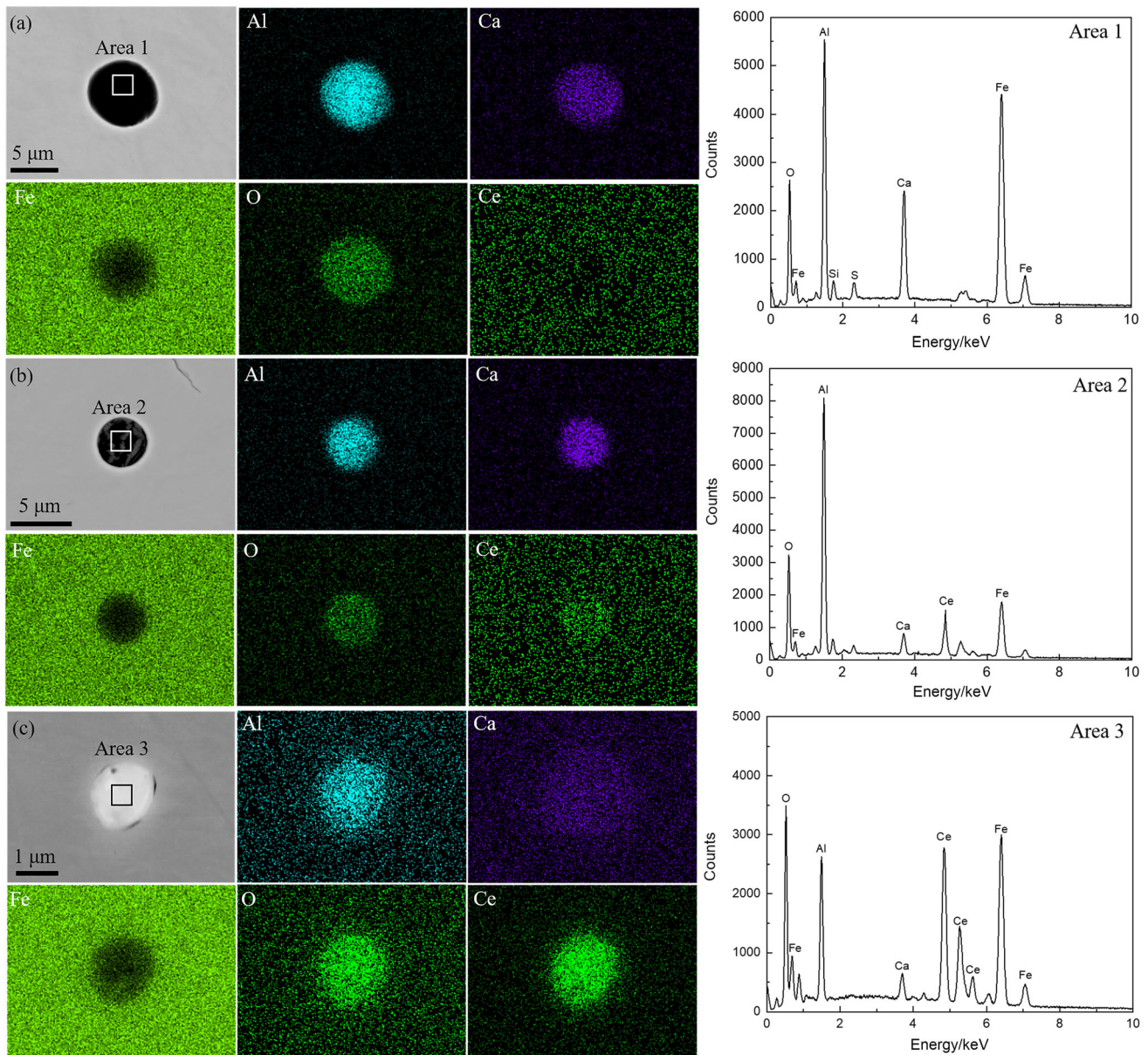


Fig. 7 Typical inclusions in No. 1 steel. **a** $\text{Al}_2\text{O}_3\text{-CaO}$ at 1 min; **b** $\text{CeAl}_{11}\text{O}_{18}\text{-CaO}$ at 5 min; **c** $\text{CeAlO}_3\text{-CaO}$ at 10 min

inclusions, the average diameter of inclusions decreased rapidly after adding cerium for 1 min and had little change with time, and this phenomenon indicated that the transient evolution of cerium-containing inclusions in the molten steel had little effect on the size of inclusions. During the cooling process, the average diameter of inclusions in No. 1 and No. 2 steels increased significantly. It was because the addition of less cerium in No. 1 steel mainly modified oxide inclusions, but did not affect MnS inclusions in the steel. As a result, MnS inclusions precipitated and wrapped several small oxide inclusions during the cooling process, resulting in the formation of larger-size inclusions in the

ingot, as shown in Fig. 16a. According to Fig. 16b, compared with other cerium-containing inclusions, CeAlO_3 inclusions were more likely to polymerize during the cooling process, forming larger inclusions and resulting in a significant increase in the average size of inclusions in No. 2 steel ingot.

Figure 15b shows the variation in the number density of inclusions in the solid steel with varied additions of cerium. With the addition of 28×10^{-6} cerium (No. 1 steel), a small number of cerium only modified oxide inclusions in the steel, so that the number density of inclusions in the steel did not change significantly. When

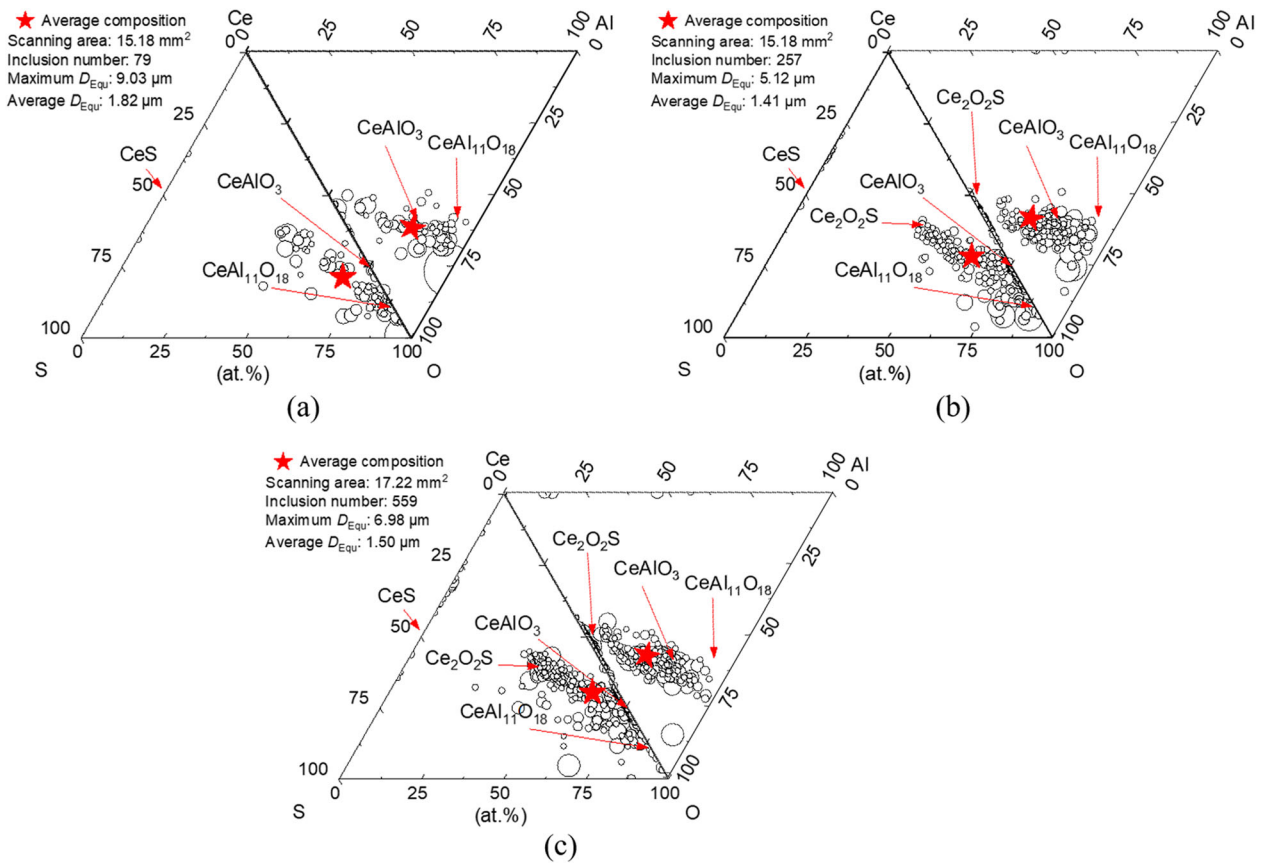


Fig. 8 Composition and size of inclusions at different time after cerium addition in No. 2 steel. **a** 1 min; **b** 5 min; **c** 10 min

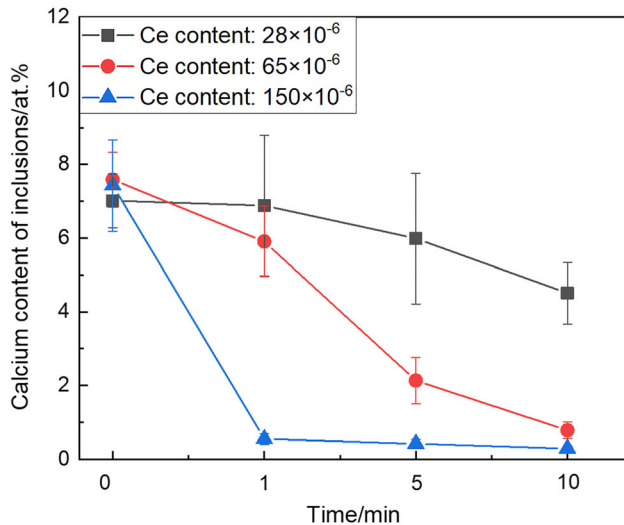


Fig. 9 Variation in calcium content of inclusions after cerium addition

the amount of cerium reached 65×10^{-6} , cerium began to combine with sulfur in the steel to produce a small number of $\text{Ce}_2\text{O}_2\text{S}$ and the number density of inclusions

increased with time. However, the number density of inclusions decreased due to the collision and polymerization of inclusions during the cooling process. In the steel with the TCe content of 150×10^{-6} , a large number of small-size $\text{Ce}_2\text{O}_2\text{S}$ inclusions in the steel increased significantly after adding cerium for 1 min, but decreased slightly after adding cerium for 5 min, because a small number of CeS– $\text{Ce}_2\text{O}_2\text{S}$ complex inclusions were generated. With the gradual homogenization of cerium in the molten steel, a large number of $\text{Ce}_2\text{O}_2\text{S}$ inclusions were produced again, resulting in an increase in the number density of inclusions. According to the change of the average size of inclusions in Fig. 15a, the collision polymerization of $\text{Ce}_2\text{O}_2\text{S}$ inclusions during the cooling process was obviously weaker than that of CeAlO_3 inclusions. The main reason for the failure of bearing steel under high cycle fatigue was subsurface cracks caused by subsurface inclusions [28–31], and the inclusion size was one of the most important factors affecting the fatigue performance of bearing steels [32, 33]. As shown in Fig. 15a, when the content of cerium was controlled at about 150×10^{-6} , the inclusion size in steel was the minimum.

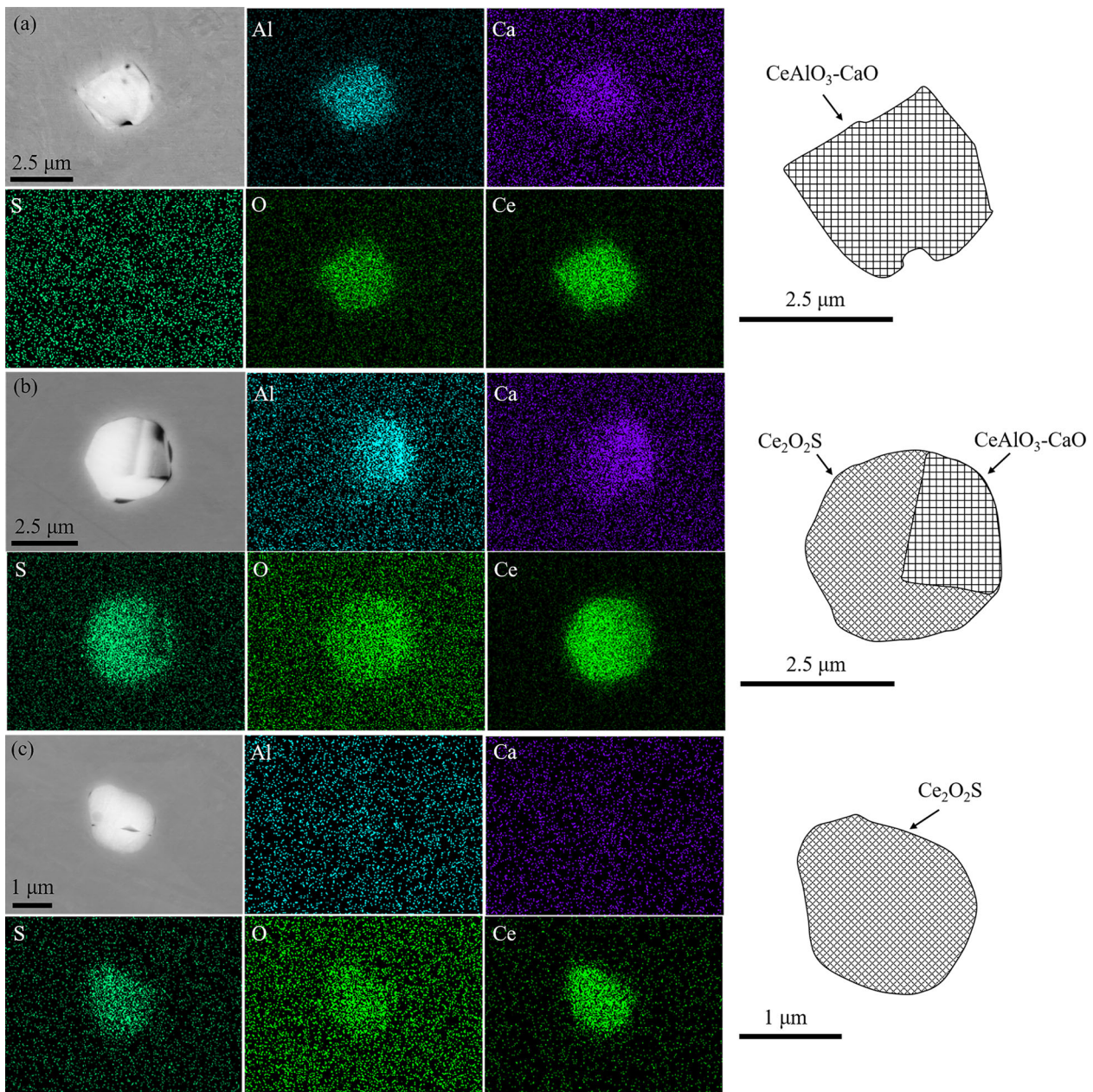


Fig. 10 Typical inclusions in No. 2 steel. **a** $\text{CeAlO}_3\text{-CaO}$ at 1 min; **b** $\text{CeAlO}_3\text{-CaO}$ and $\text{Ce}_2\text{O}_2\text{S}$ complex inclusion at 5 min; **c** $\text{Ce}_2\text{O}_2\text{S}$ at 10 min

5 Thermodynamic analysis of inclusions formation in steel

Thermodynamic software FactSage 7.1 was used to calculate the phase diagram of solid inclusions in the steel at 1600 °C using databases of FactPS, FToxide and FTmisc. The thermodynamic data of $\text{Ce}_2\text{O}_2\text{S}$ came from Vahed and Key in 1976 [34], and the influence of calcium was not considered in the calculation process due to the low calcium content in the steel. As shown in Fig. 17, the

evolution sequence of inclusions in the steel with the variation of the TCe content at 1600 °C was: $\text{Al}_2\text{O}_3 \rightarrow \text{CeAl}_{11}\text{O}_{18} \rightarrow \text{CeAlO}_3 \rightarrow \text{Ce}_2\text{O}_2\text{S}$. Dotted lines in Fig. 17 were contents of TCe in No. 1, No. 2 and No. 3 steels, respectively. By comparing the evolution sequence of inclusions in the molten steel in Figs. 6, 8 and 11, the calculated result was consistent with the experimental result.

Figure 18 shows the phase stability diagram of inclusions as a function of the dissolved cerium ($[\text{Ce}]$) and the

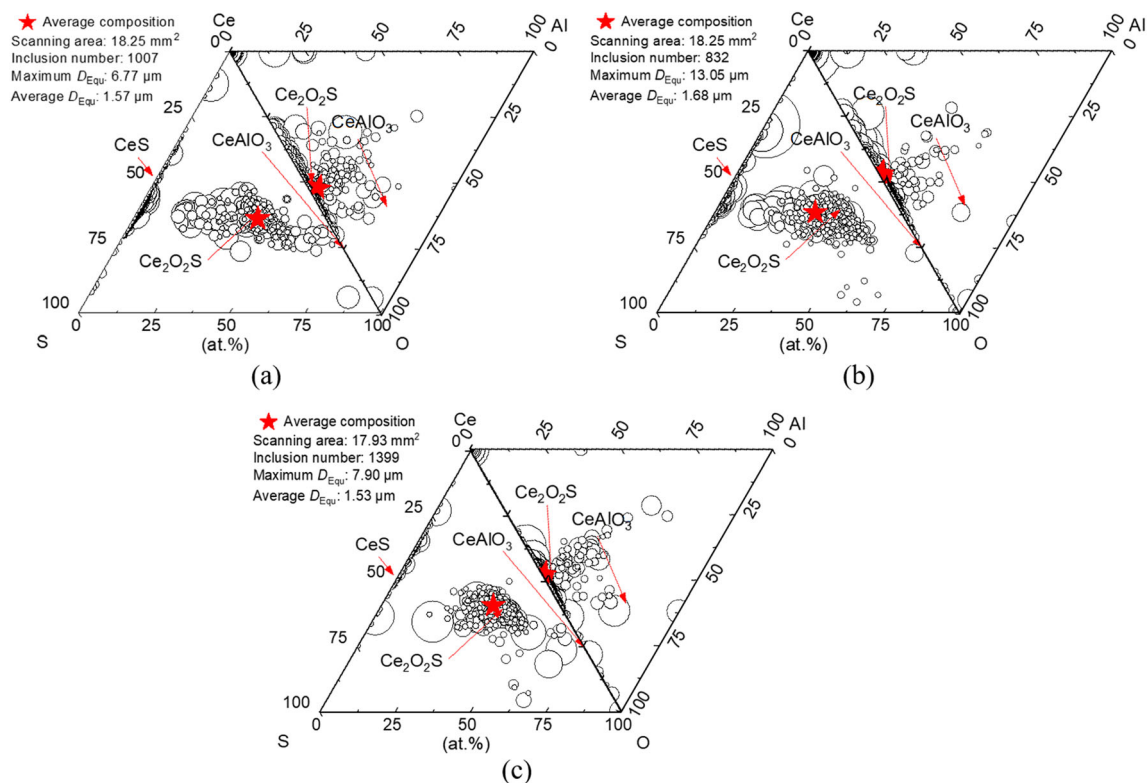


Fig. 11 Composition and size of inclusions at different time after cerium addition in No. 3 steel. **a** 1 min; **b** 5 min; **c** 10 min

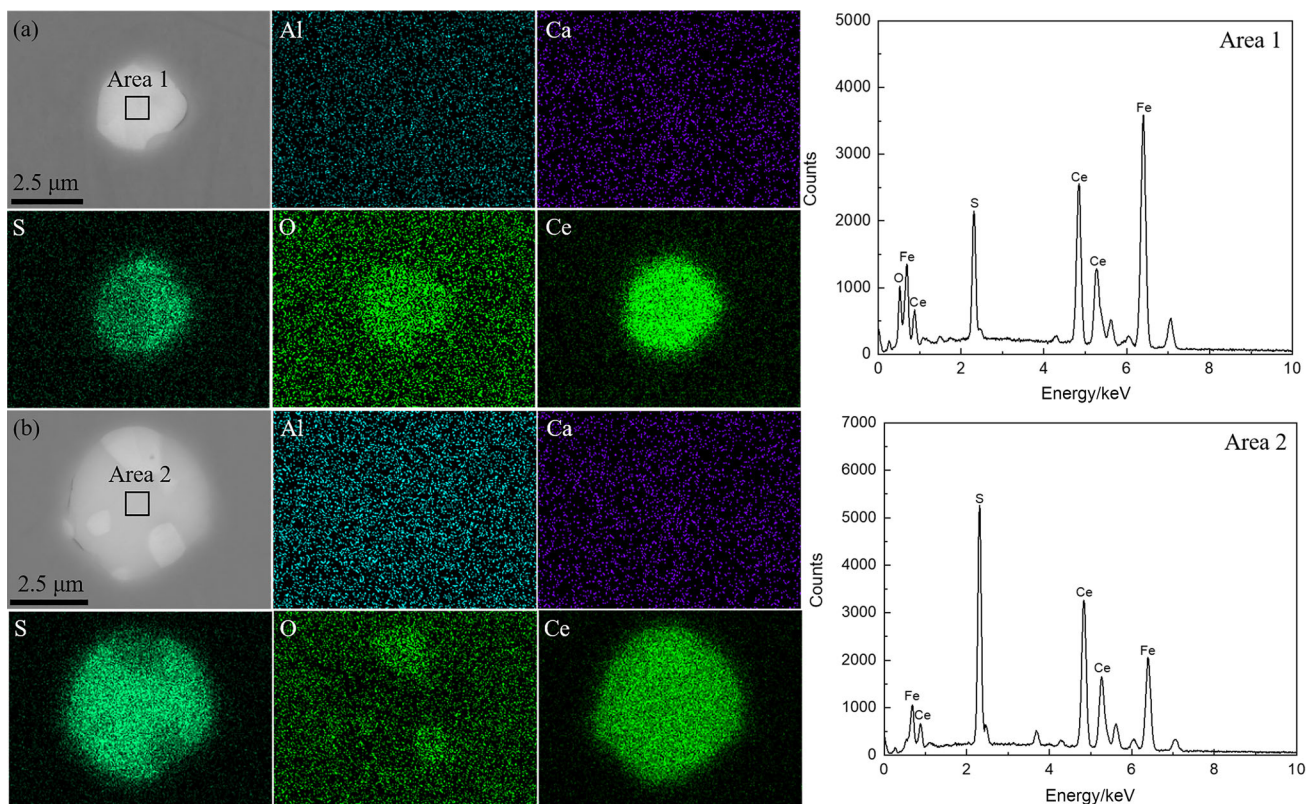


Fig. 12 Typical inclusions in No. 3 steel. **a** $\text{Ce}_2\text{O}_2\text{S}$ and CeS complex inclusion at 5 min; **b** $\text{Ce}_2\text{O}_2\text{S}$ at 10 min

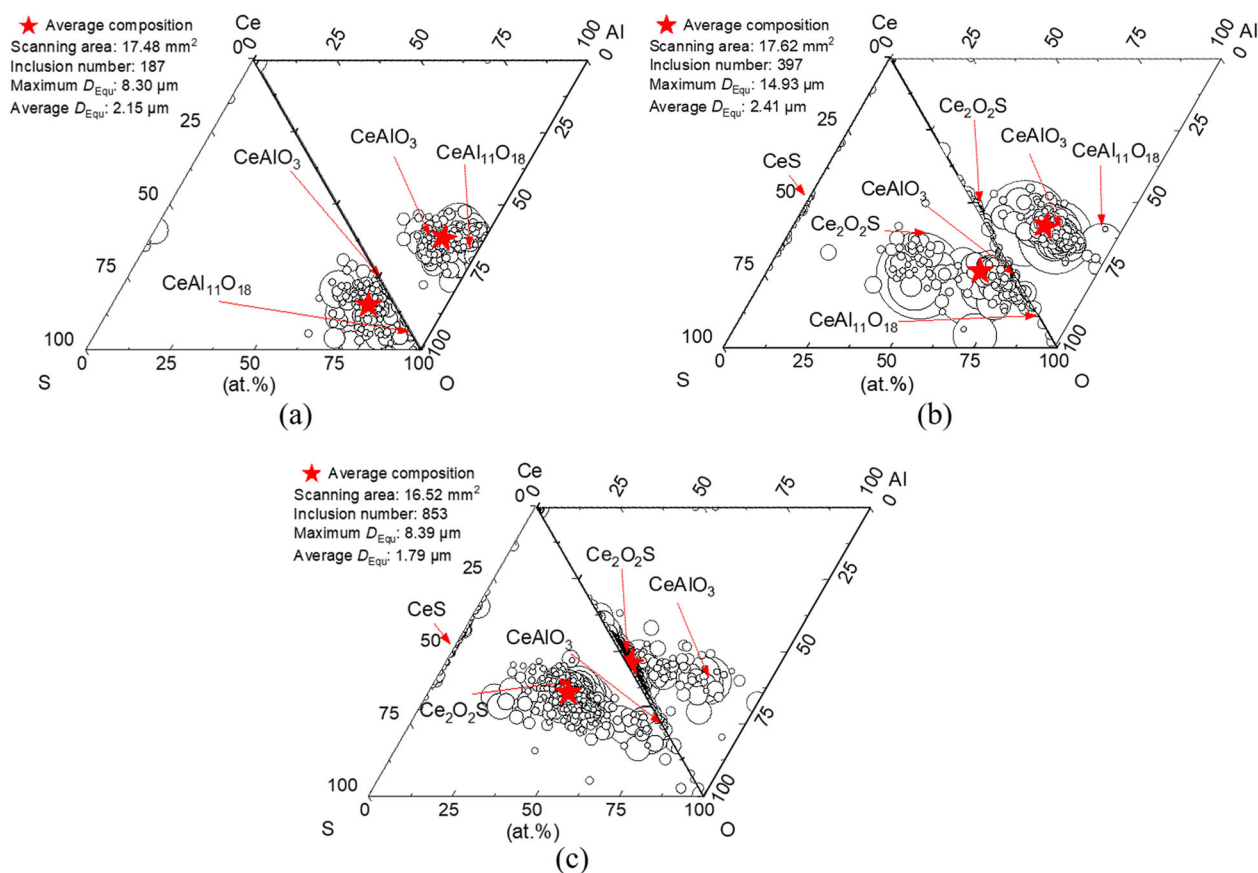
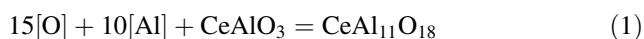


Fig. 13 Composition and size of inclusions in ingots. **a** No. 1 steel; **b** No. 2 steel; **c** No. 3 steel

dissolved aluminum ([Al]) at different contents of dissolved oxygen ([O]). The same database was used for calculation as Fig. 17. According to the experimental result, the content of [Ce] and [Al] in the steel was much smaller than that of TCe and TAl. Therefore, the amount of cerium was lower, and cerium and aluminum in the steel mainly existed in the form of inclusions, which was similar to the occurrence state of calcium in the steel [35, 36].

Calculation of inclusions transformation during the cooling process was performed using FactPS, FToxid and FSstel databases, and the result is shown in Fig. 19. With the decrease in temperature, the metastable $\text{CeAl}_{11}\text{O}_{18}$ inclusions changed to stable Al_2O_3 and CeAlO_3 at 1376.9 °C. The reaction speculation is shown in Eqs. (1) and (2), which were consistent with the experimental result, as shown in Figs. 7b and 14a.



6 Conclusions

1. With the increase in the cerium content from 0 to 150×10^{-6} , the modification sequence of inclusions in the molten high-carbon chromium bearing steel was as follows: $\text{Al}_2\text{O}_3 \rightarrow \text{CeAl}_{11}\text{O}_{18} \rightarrow \text{CeAlO}_3 \rightarrow \text{Ce}_2\text{O}_2\text{S}$, and the trace CaO in inclusions changed to [Ca] when CeAlO_3 changed to $\text{Ce}_2\text{O}_2\text{S}$.
2. When the amount of cerium was 28×10^{-6} , $\text{CeAl}_{11}\text{O}_{18}$ inclusions in the molten steel were transformed into Al_2O_3 and CeAlO_3 inclusions during the cooling process.
3. After the addition of cerium, initial Al_2O_3 inclusions in the steel were modified into smaller cerium-containing inclusions. The precipitation of MnS and collision polymerization of CeAlO_3 resulted in the increase in the average size of inclusions during the solidification of No. 1 and No. 2 steels. Therefore, the target inclusion modified by cerium to achieve a better fatigue performance of bearing steel should be $\text{Ce}_2\text{O}_2\text{S}$.

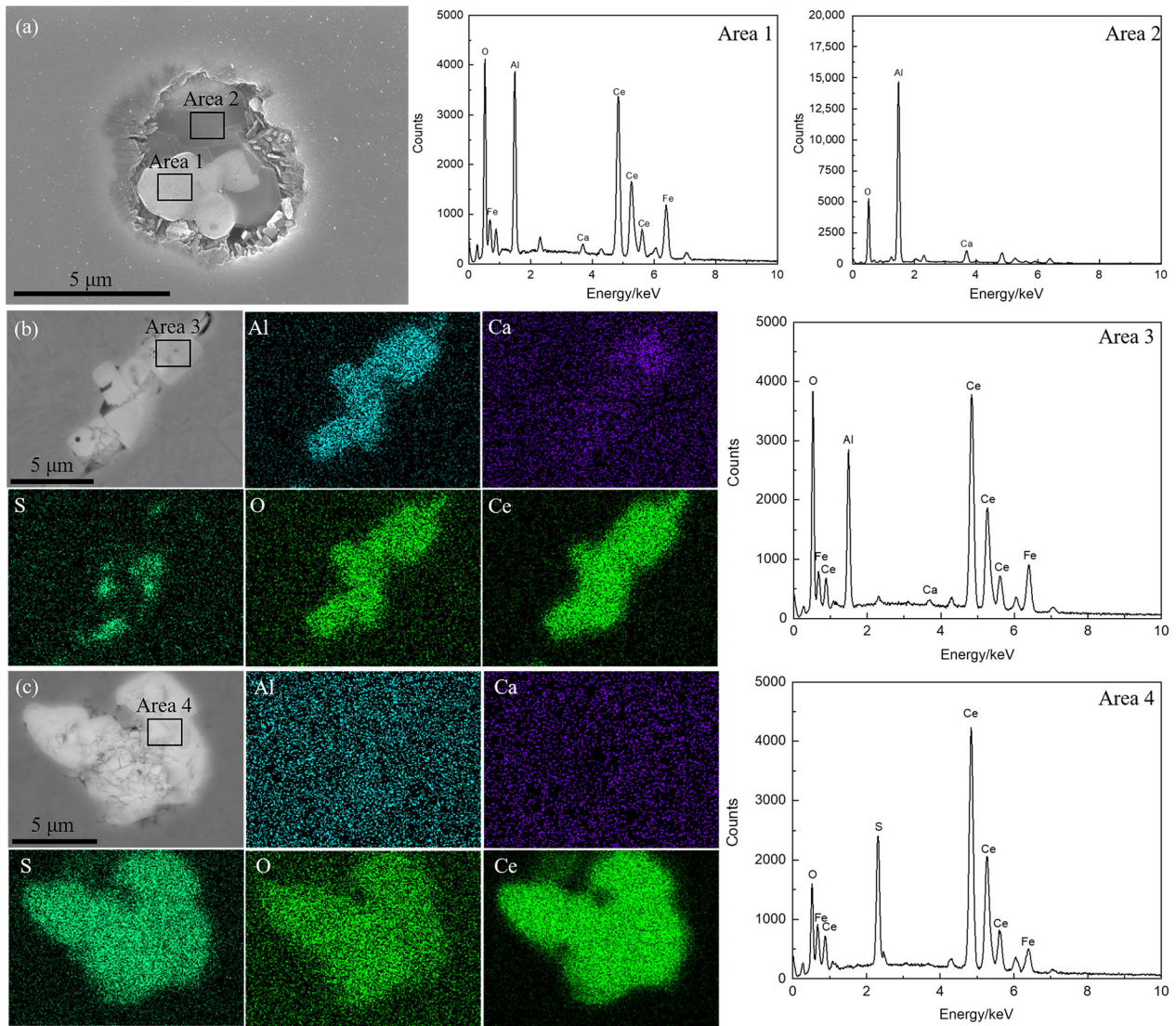


Fig. 14 Typical inclusions in solidified and cooled ingot. **a** Al₂O₃ and CeAlO₃ complex inclusion in No. 1 steel; **b** CeAlO₃ inclusion in No. 2 steel; **c** Ce₂O₂S inclusion in No. 3 steel

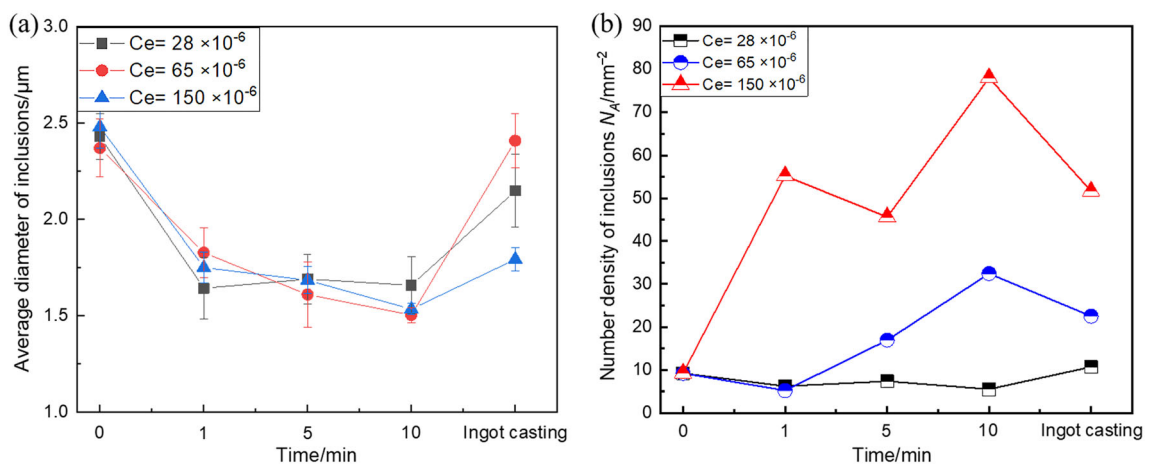


Fig. 15 Variation of average diameter of inclusions (**a**) and number density of inclusions (**b**) after cerium additions

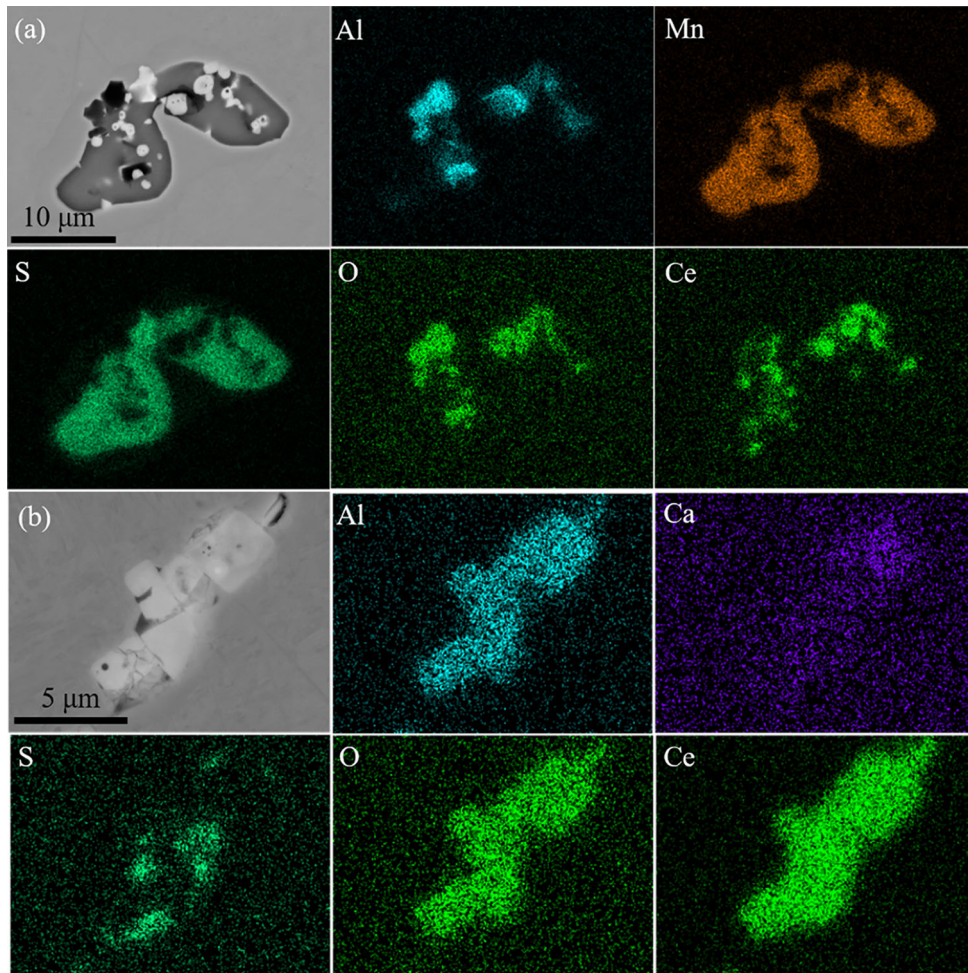


Fig. 16 Polymerization of inclusions during cooling process. **a** No. 1 steel; **b** No. 2 steel

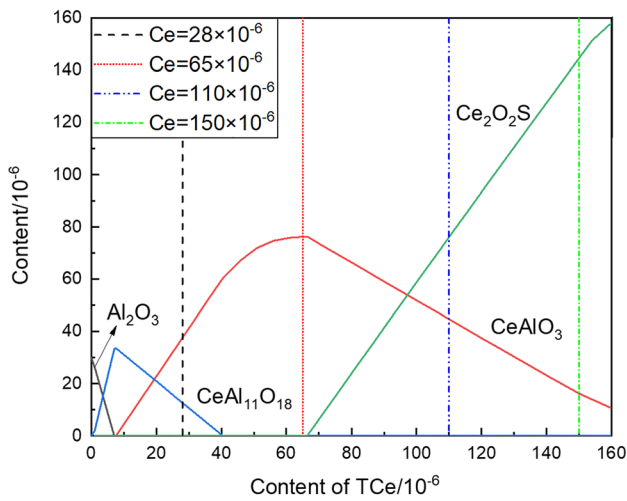


Fig. 17 Phase equilibrium diagram of solid inclusion at 1600 °C

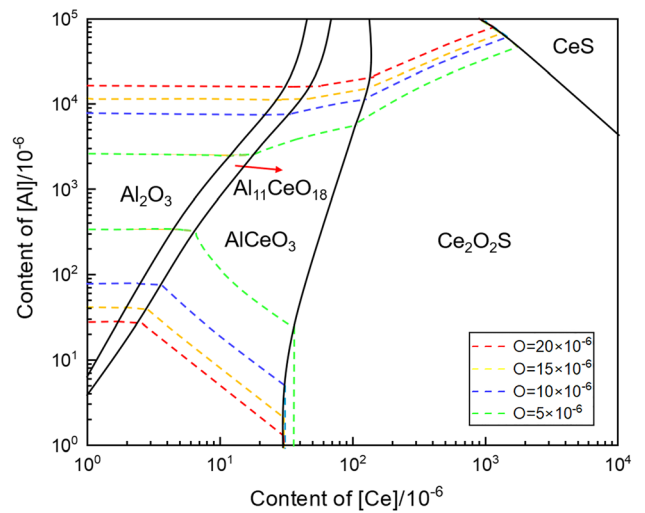


Fig. 18 Phase stability diagram of inclusions as a function of [Ce] and [Al]

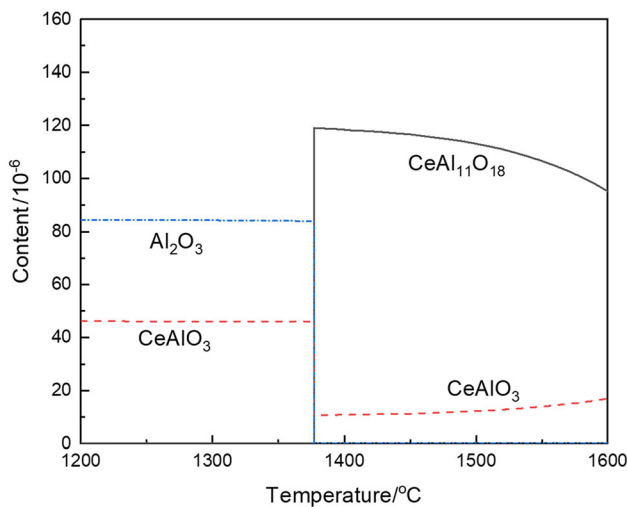


Fig. 19 Transformation of inclusions in No. 1 steel during solidification and cooling process

Acknowledgements The authors are grateful for the support from the Natural Science Foundation of Hebei Province (Grant No. E2021203062), S&T Program of Hebei (Grant No. 20311006D) and the High Steel Center (HSC) at North China University of Technology, Yanshan University and University of Science and Technology Beijing.

Declarations

Conflict of interest The authors have no competing interests to declare that are relevant to the content of this article.

References

- [1] H. Bhadeshia, *Prog. Mater. Sci.* 57 (2012) 268–435.
- [2] P. Wang, B. Wang, Y. Liu, P. Zhang, Y. Luan, D. Li, Z. Zhang, *Scripta Mater.* 206 (2022) 114232.
- [3] K. Hashimoto, T. Fujimatsu, N. Tsunekage, K. Hiraoka, K. Kida, E.C. Santos, *Mater. Des.* 32 (2011) 1605–1611.
- [4] J. Guan, L. Wang, C. Zhang, X. Ma, *Tribol. Int.* 106 (2017) 123–131.
- [5] S.M. Moghaddam, F. Sadeghi, K. Paulson, N. Weinzapfel, M. Correns, V. Bakolas, M. Dinkel, *Int. J. Fatigue* 80 (2015) 203–215.
- [6] K. Hashimoto, K. Hiraoka, K. Kida, E. Costa Santos, *Mater. Sci. Technol.* 28 (2012) 39–43.
- [7] D. Priestersbach, P. Grad, E. Kerscher, *Int. J. Fatigue* 64 (2014) 114–120.
- [8] Z. Cao, Z. Shi, F. Yu, G. Wu, W. Cao, Y. Weng, *Int. J. Fatigue* 126 (2019) 1–5.
- [9] Y. Yamashita, Y. Murakami, *Int. J. Fatigue* 93 (2016) 406–414.
- [10] G. Donzella, M. Faccoli, A. Mazzù, C. Petrogalli, H. Desimone, *Eng. Fract. Mech.* 78 (2011) 2761–2774.
- [11] H. Li, Y. Yu, X. Ren, S. Zhang, S. Wang, *J. Iron Steel Res. Int.* 24 (2017) 925–934.
- [12] Z. Shaohua, Y. Yanchong, W. Shebin, L. Hao, *J. Rare Earths* 35 (2017) 518–524.
- [13] Q. Ren, L. Zhang, *Metall. Mater. Trans. B* 51 (2020) 589–600.
- [14] Q. Ren, L. Zhang, Y. Liu, L. Cui, W. Yang, *J. Mater. Res. Technol.* 9 (2020) 8197–8206.
- [15] C. Yang, Y. Luan, D. Li, Y. Li, *Int. J. Fatigue* 116 (2018) 396–408.
- [16] Y. Liu, Z. Yang, Y. Li, S. Chen, S. Li, W. Hui, Y. Weng, *Mater. Sci. Eng. A* 517 (2009) 180–184.
- [17] H. Mayer, W. Haydn, R. Schuller, S. Issler, B. Furtner, M. Bacher-Höchst, *Int. J. Fatigue* 31 (2009) 242–249.
- [18] A. Katsumata, H. Todoroki, *Iron Steelmak.* 29 (2002) 51–57.
- [19] Q. Wang, L. Wang, Y. Liu, K. Chou, *J. Min. Metall. B Metall.* 53 (2017) 365–372.
- [20] H. Wang, S. Jiang, P. Yu, L. Sun, Y. Wang, *ISIJ Int.* 60 (2020) 2316–2324.
- [21] Y. Meng, C. Yan, X. Yang, X. Ju, *ISIJ Int.* 60 (2020) 534–538.
- [22] S. Imashuku, K. Wagatsuma, *Metall. Mater. Trans. B* 51 (2020) 79–84.
- [23] X.Y. Wu, B.B. Liu, Q.R. Tian, J.B. Xie, J.X. Fu, *Trans. Indian Inst. Met.* 75 (2022) 2031–2039.
- [24] X. Wang, G. Li, Y. Liu, F. Wang, Q. Wang, *ISIJ Int.* 61 (2021) 1850–1859.
- [25] C. Yang, Y. Luan, D. Li, Y. Li, *J. Mater. Sci. Technol.* 35 (2019) 1298–1308.
- [26] C. Yang, Y. Luan, D. Li, Y. Li, *Int. J. Fatigue* 131 (2020) 105263.
- [27] J. Wang, W. Li, Y. Ren, L. Zhang, *Steel Res. Int.* 90 (2019) 1800600.
- [28] J.J. Hoo, Effect of steel manufacturing processes on the quality of bearing steels, ASTM International, Pennsylvania, USA, 1988.
- [29] Y. Murakami, *Int. J. Fatigue* 3 (1994) 345–351.
- [30] J. Monnot, B. Heritier, J.Y. Cogne, Relationship of melting practice, inclusion type, and size with fatigue resistance of bearing steels, ASTM International, Pennsylvania, USA, 1988.
- [31] T. Sakai, Y. Sato, N. Oguma, *Fatig. Fract. Eng. Mater. Struct.* 25 (2002) 765–773.
- [32] K. Hashimoto, T. Fujimatsu, N. Tsunekage, K. Hiraoka, K. Kida, E.C. Santos, *Mater. Des.* 32 (2011) 4980–4985.
- [33] S.M. Moghaddam, F. Sadeghi, *Tribol. Trans.* 59 (2016) 1142–1156.
- [34] A. Vahed, D. Kay, *Metall. Trans. B* 7 (1976) 375–383.
- [35] Y. Liu, L. Zhang, *Metall. Mater. Trans. B* 49 (2018) 1624–1631.
- [36] N. Verma, P.C. Pistorius, R.J. Fruehan, M.S. Potter, H.G. Oltmann, E.B. Pretorius, *Metall. Mater. Trans. B* 43 (2012) 830–840.

Springer Nature or its licensor (e.g. a society or other partner) holds exclusive rights to this article under a publishing agreement with the author(s) or other rightsholder(s); author self-archiving of the accepted manuscript version of this article is solely governed by the terms of such publishing agreement and applicable law.